J. Fluid Mech. (1980), *vol.* 100, *part* 4, *pp.* 817–829
Printed in Great Britain

Incompressible flow in a labyrinth seal

By H. STOFF

Chaire de la Mécanique de la Turbulence
and Institut de Thermique Appliquée,
Ecole Polytechnique Fédérale de Lausanne

(Received 19 April 1979 and in revised form 19 February 1980)

The incompressible flow in a labyrinth seal is computed using the 'k–ϵ' turbulence model with a pressure–velocity computer code in order to explain leakage phenomena against the mean pressure gradient. The flow is axisymmetric between a rotating shaft and an enclosing cylinder at rest. The main stream in circumferential direction induces a secondary mean flow vortex pattern inside annular cavities on the surface of the shaft. The domain of interest is one such cavity of an enlarged model of a labyrinth seal, where the finite difference result of a computer program is compared with measurements obtained by a back-scattering laser-Doppler anemometer at a cavity Reynolds number of $\sim 3 \times 10^4$ and a Taylor number of $\sim 1{\cdot}2 \times 10^4$. The turbulent kinetic energy and the turbulence dissipation rate are verified experimentally for a comparison with the result of the turbulence model.

1. Introduction

Labyrinth seals are fitted into a mechanical installation in order to prevent friction between the casing and the shaft at high revving. With an imposed pressure gradient along the shaft, it is possible to generate an axial flow which should prevent mass transfer from a downstream location in the upstream direction. In spite of the presence of such an imposed fluid barrier, it has been found in some cases that transport of matter (e.g. oil or vapour droplets) may occur. The subject of this study has been to compute the flow pattern and to consider the effect of turbulence on the mean flow field.

2. The experimental installation

The real scale size of the labyrinth under consideration is too small for the measurement of velocity profiles. This is the reason why the present study concentrates on the enlarged model of Boyman & Suter (1978) following the similarity conditions of Reynolds and Taylor with water as operating fluid. The shaft, with five baffles separating four annular chambers of the labyrinth, rotates about its vertical axis inside a smooth cylinder. A Plexiglas window allows for optical measurements in the domain. The leakage flux mounts along the shaft. Its flow rate is checked with a rotameter. The computational domain consists of one of the annular cavities between the baffles (figure 1) with a gap-to-radius ratio of $d/r \approx 0{\cdot}1$. In a turbomachine the

Present address: Brown Boveri & Co., Ltd., Dept. TCT-13, CH-5401 Baden, Switzerland.

0022-1120/80/4551-1940 $02.00

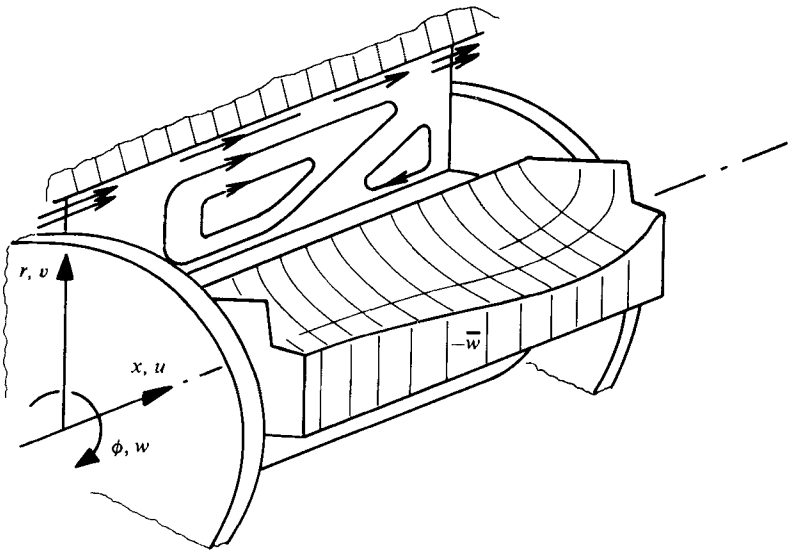

FIGURE 1. Schematic view of the flow configuration around the shaft at one cell of the labyrinth with the shape of the mean circumferential velocity profile ($\bar{w}$) and the recirculation flow pattern in a constant ϕ plane.

size of this value is imposed by considerations concerning the mechanical vibrations of the shaft. Laser–Doppler measurements exhibit the following features of the flow pattern.

(i) The circumferential bulk velocity W_0 is about 0·65 times the speed of the shaft which is, due to the baffles, superior to the value of 0·5 for the rotating Couette flow between a smooth shaft and an enclosing cylinder (Taylor 1935).

(ii) The inlet velocity in the axial direction at the passage over the baffles is defined by the operating conditions for a real size machine as 0·036 times the circumferential velocity of the shaft. A double helix with meridional velocities of up to 10 % of the rotational speed of the shaft occupies the chamber between the baffles.

The conditions of the flow are thus characterized by the Reynolds and the Taylor number based on the bulk velocity W_0, the kinematic viscosity ν, the radius r of the shaft, and the distance d between the bottom of the cavity and the enclosing cylinder;

$$Re_{\text{cavity}} = \frac{W_0 d}{\nu} \approx 3 \times 10^4; \quad Ta = \frac{W_0 d}{\nu}\left(\frac{d}{r}\right)^{\frac{1}{2}} \approx 10^4.$$

3. The basic equations

For the axisymmetric installation the computation may be reduced to a two-dimensional problem with three velocity components, the circumferential derivative $\partial(\,)/\partial\phi$ being zero.

The Taylor number in this case is of the order of 10 times the critical value. In the work of Swinney, Gollub & Fenstermacher it is suggested that turbulence does not occur until 400 times the critical value of the Taylor number, and that the velocity fluctuations are rather due to vortex waves than to turbulence (Gollub & Swinney 1975; Haken 1977). The present investigation does not include a detailed study

Continuity equation

$$\frac{\partial(\rho r\bar{u})}{\partial x}+\frac{\partial(\rho r\bar{v})}{\partial r}+\frac{\partial(\rho\bar{w})}{\partial\phi}=0 \quad \left(\frac{\partial}{\partial\phi}=0\right). \tag{1}$$

Momentum equations

$$\rho\left[\bar{u}\frac{\partial\bar{u}}{\partial x}+\bar{v}\frac{\partial\bar{u}}{\partial r}+\frac{\bar{w}}{r}\frac{\partial\bar{u}}{\partial\phi}\right]=-\frac{\partial\bar{p}}{\partial x}+\left[\frac{\partial}{\partial x}\mu\frac{\partial\bar{u}}{\partial x}+\frac{\partial}{\partial r}\mu\frac{\partial\bar{u}}{\partial r}+\frac{\mu}{r}\frac{\partial\bar{u}}{\partial r}+\frac{1}{r^2}\frac{\partial}{\partial\phi}\mu\frac{\partial\bar{u}}{\partial\phi}\right]$$
$$-\rho\left[\frac{\partial\overline{u'u'}}{\partial x}+\frac{1}{r}\frac{\partial r\overline{u'v'}}{\partial r}+\frac{1}{r}\frac{\partial\overline{u'w'}}{\partial\phi}\right], \tag{2}$$

$$\rho\left[\bar{u}\frac{\partial\bar{v}}{\partial x}+\bar{v}\frac{\partial\bar{v}}{\partial r}+\frac{\bar{w}}{r}\frac{\partial\bar{v}}{\partial\phi}-\frac{\bar{w}^2}{r}\right]=-\frac{\partial\bar{p}}{\partial r}+\left[\frac{\partial}{\partial x}\mu\frac{\partial\bar{v}}{\partial x}+\frac{\partial}{\partial r}\mu\frac{\partial\bar{v}}{\partial r}+\frac{\mu}{r}\frac{\partial v}{\partial r}+\frac{1}{r^2}\frac{\partial}{\partial\phi}\mu\frac{\partial\bar{v}}{\partial\phi}-\frac{\mu\bar{v}}{r^2}-\frac{2\mu}{r^2}\frac{\partial\bar{w}}{\partial\phi}\right]$$
$$-\rho\left[\frac{\partial\overline{u'v'}}{\partial x}+\frac{1}{r}\frac{\partial r\overline{v'v'}}{\partial r}+\frac{1}{r}\frac{\partial\overline{v'w'}}{\partial\phi}-\frac{\overline{w'^2}}{r}\right], \tag{3}$$

$$\rho\left[\bar{u}\frac{\partial\bar{w}}{\partial x}+\bar{v}\frac{\partial\bar{w}}{\partial r}+\frac{\bar{w}}{r}\frac{\partial\bar{w}}{\partial\phi}+\frac{\overline{vw}}{r}\right]=-\frac{1}{r}\frac{\partial\bar{p}}{\partial\phi}+\left[\frac{\partial}{\partial x}\mu\frac{\partial\bar{w}}{\partial x}+\frac{\partial}{\partial r}\mu\frac{\partial\bar{w}}{\partial r}+\frac{\mu}{r}\frac{\partial\bar{w}}{\partial r}+\frac{\bar{w}}{r}\frac{\partial\mu}{\partial r}+\frac{1}{r^2}\frac{\partial}{\partial\phi}\mu\frac{\partial\bar{w}}{\partial\phi}-\frac{\mu\bar{w}}{r^2}+\frac{2\mu}{r^2}\frac{\partial\bar{v}}{\partial\phi}\right]$$
$$-\rho\left[\frac{\partial\overline{u'w'}}{\partial x}+\frac{1}{r}\frac{\partial r\overline{v'w'}}{\partial r}+\frac{1}{r}\frac{\partial\overline{w'w'}}{\partial\phi}+\frac{\overline{v'w}}{r}\right]. \tag{4}$$

convection — diffusion

TABLE 1. Mean continuity and momentum equations for the steady axisymmetric flow in the labyrinth.

about the form of the fine-scale motion over a range of Taylor numbers. The tangential velocity auto-correlation functions, measured in circumferential direction from 50–200 % of the nominal rotational speed, exhibit a shape of the kinetic energy spectrum comparable to turbulence. Therefore a turbulence model should be apt of describing the effect of the fluctuating kinetic energy on the mean momentum, regardless of a wave-like or a turbulent character of the motion. With the effect of the fluctuations accounted for by the turbulence model, the set of equations for the transport of mean flow quantities reduces further to the steady-state form with $\partial(\ )/\partial t = 0$. The system of equations to be solved for this problem is given in table 1, equations (1)–(4). A solution is achieved with the set of flow equations in table 2 used also by Gosman *et al.* (1976), Hutchinson *et al.* (1976) and Lilley (1976), consisting of the continuity equation (5), three momentum equations (6), (7) and (8) for the mean velocity components $(\bar{u}, \bar{v}, \bar{w})$ in two dimensions. Additional information for the velocity fluctuations (u', v', w') is provided by a two-equation turbulence model.

A closure with a simple algebraic expression for an effective viscosity based on the shear stress, causes the turbulence diffusion to decrease too rapidly outside the boundary layers. In such a computation the helical movement in the meridional plane does not coincide with the experimental observations. A transport equation can carry turbulence energy outside the regions of strong shear towards the centre of the domain. A second transport equation for the variations in the turbulence dissipation replaces the need for a suitable flow-dependent dissipation scale. The original form of the Saffman two-equation model gives too low values for the effective viscosity. Satisfactory results are computed with the 'k–ϵ' model in the form given by Gosman & Pun (1974). Therefore the transport of two more quantities is incorporated into the system

$$\frac{\partial(\rho r\bar{u})}{\partial x}+\frac{\partial(\rho r\bar{v})}{\partial r}=0, \tag{5}$$

$$\frac{1}{r}\left[\frac{\partial(\rho r\overline{uu})}{\partial x}+\frac{\partial(\rho r\overline{vu})}{\partial r}-\frac{\partial}{\partial x}r\mu_e\frac{\partial\bar{u}}{\partial x}-\frac{\partial}{\partial r}r\mu_e\frac{\partial\bar{u}}{\partial r}\right]=-\frac{\partial\bar{p}}{\partial x}, \tag{6}$$

$$\frac{1}{r}\left[\frac{\partial(\rho r\overline{uv})}{\partial x}+\frac{\partial(\rho r\overline{vv})}{\partial r}-\frac{\partial}{\partial x}r\mu_e\frac{\partial\bar{v}}{\partial x}-\frac{\partial}{\partial r}r\mu_e\frac{\partial\bar{v}}{\partial r}\right]=-\frac{\partial\bar{p}}{\partial r}-\frac{\mu_e\bar{v}}{r^2}+\frac{\rho\overline{w^2}}{r}, \tag{7}$$

$$\frac{1}{r}\left[\frac{\partial(\rho r\overline{uw})}{\partial x}+\frac{\partial(\rho r\overline{vw})}{\partial r}-\frac{\partial}{\partial x}r\mu_e\frac{\partial\bar{w}}{\partial x}-\frac{\partial}{\partial r}r\mu_e\frac{\partial\bar{w}}{\partial r}\right]=-\frac{\mu_e\bar{w}}{r^2}+\frac{\bar{w}}{r}\frac{\partial\mu_e}{\partial r}-\frac{\rho\overline{(vw)}}{r}, \tag{8}$$

$$\mu_e=c_\mu\rho\frac{q^4}{4\epsilon}, \tag{9}$$

$$\frac{1}{r}\left[\frac{\partial(\rho r\bar{u}q^2)}{\partial x}+\frac{\partial(\rho r\bar{v}q^2)}{\partial r}-\frac{\partial}{\partial x}\left(\frac{r\mu_e}{\sigma_q}\frac{\partial q^2}{\partial x}\right)-\frac{\partial}{\partial r}\left(\frac{r\mu_e}{\sigma_q}\frac{\partial q^2}{\partial r}\right)\right]=G-c_D\rho\epsilon, \tag{10}$$

$$\frac{1}{r}\left[\frac{\partial(\rho r\bar{u}\epsilon)}{\partial x}+\frac{\partial(\rho r\bar{v}\epsilon)}{\partial r}-\frac{\partial}{\partial x}\left(\frac{r\mu_e}{\sigma_\epsilon}\frac{\partial\epsilon}{\partial x}\right)-\frac{\partial}{\partial r}\left(\frac{r\mu_e}{\sigma_\epsilon}\frac{\partial\epsilon}{\partial r}\right)\right]=c_1\frac{\epsilon G}{q^2}-c_2\rho\frac{\epsilon^2}{q^2}, \tag{11}$$

$$G=\mu_e\left[2\left[\left(\frac{\partial\bar{u}}{\partial x}\right)^2+\left(\frac{\partial\bar{v}}{\partial r}\right)^2+\left(\frac{\bar{v}}{r}\right)^2\right]+\left(\frac{\partial\bar{u}}{\partial r}+\frac{\partial\bar{v}}{\partial x}\right)^2+\left(\frac{\partial\bar{w}}{\partial x}\right)^2+\left(\frac{\partial\bar{w}}{\partial r}-\frac{\bar{w}}{r}\right)^2\right].$$

$c_\mu=0{\cdot}09;\ \sigma_q=1;\ \sigma_\epsilon=1{\cdot}21;\ c_D=1;\ c_1=1{\cdot}44;\ c_2=1{\cdot}92$

TABLE 2. The equations solved in the computer program.

of nonlinear equations in table 2: kinetic energy $\frac{1}{2}q^2$ and dissipation ϵ of turbulence with equations (10) and (11) respectively. The usual notation 'k–ϵ' has been changed in the following to 'q^2–ϵ' in order to retain k for the wavenumber.

For the rectangular configuration of the labyrinth, we have decided to rely on an implicit finite difference code of Gosman & Pun (1974) which has proved to be successful in similar cases (Gosman *et al.* 1976; Hutchinson *et al.* 1976; Lilley 1976). The iterative pressure–velocity procedure fulfils the incompressibility condition by means of a pressure–correction potential. With a computational grid over the whole domain, only a few points remain inside the boundary layer which is of about 10 % of the cavity width. Therefore the boundary values attributed to the points closest to the limits are very important for the success of the computation. The wall formulae used by Gosman & Pun (1974) have been adopted without changes on the stationary and the moving boundaries (table 3, equations (12)–(15)). Although the logarithmic form for the velocity profile on the spinning cylinder is certainly a crude assumption, this law gives rise to acceptable overall results. It is not possible to base the computation on more detailed measurements in the wall proximity, because the reflexions of light prohibit laser measurements inside the boundary layer close to the walls, especially on the rotating shaft. A more severe influence than the use of the logarithmic velocity law on the moving surfaces is introduced by the boundary conditions at the inlet and outlet of the computational domain. The axial velocity component $\bar{u}$ needs a fixed value at the inflow and at the outflow slot. For all other variables, good results have been achieved by feeding the iterated values for the outlet back into the inlet at the end of each iteration step. This implies the sequence of identical labyrinth chambers in a row on the shaft.

$$\text{Velocity for } y^+ > 11 \quad \frac{\Delta\bar{u}}{U_\tau} = \frac{1}{\kappa}\ln(Ey^+). \tag{12}$$

$$\text{Turbulent shear stress} \quad \tau = \frac{\rho c_\mu^{\frac{1}{4}}(q^2/2)^{\frac{1}{2}}\Delta\bar{u}\kappa}{\ln(Ey^+)}. \tag{13}$$

$$\text{Turbulence energy} \quad \frac{q^2}{2} = \frac{U_\tau^2}{c_\mu^{\frac{1}{2}}}. \tag{14}$$

$$\text{Dissipation of turbulence} \quad \epsilon = \frac{U_\tau^3}{\kappa y}. \tag{15}$$

$\Delta\bar{u}$ = velocity parallel to the wall; $U_\tau = (\tau/\rho)^{\frac{1}{2}}$ = friction velocity; y = distance from the wall; $y^+ = yU_\tau/\nu$; τ = shear stress; ρ = density; ν = kinematic viscosity; $\kappa = 0{\cdot}4187$; $E = 9{\cdot}793$; $c_\mu = 0{\cdot}09$.

TABLE 3. The solid-wall boundary conditions in the computer program.

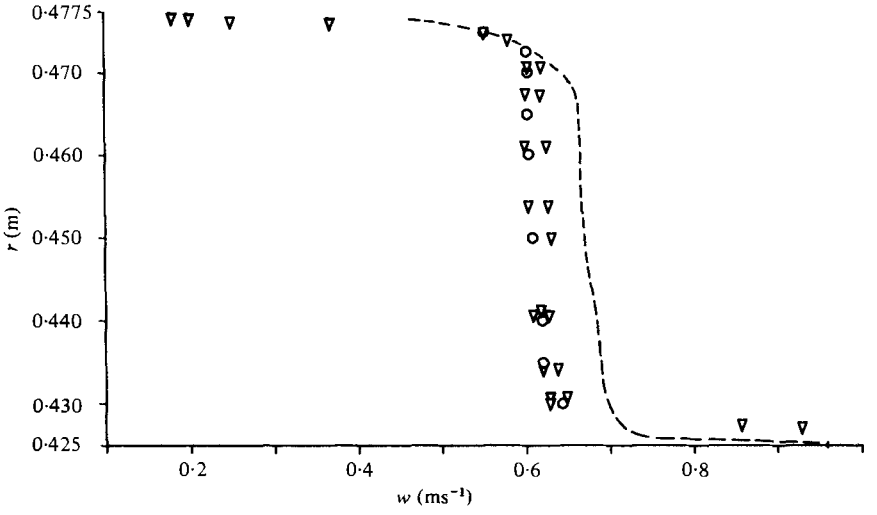

FIGURE 2. Radial distribution of the mean circumferential velocity, comparison of finite difference result (– – –) and LDA measurements (○, ▽).

4. The energy-dissipation model for the case of the labyrinth

In many of the applications of a turbulence model to a real flow, an experimental verification is made only for the turbulence energy or the shear stress, but the distribution of the dissipation rate ϵ in the flow field is just assumed. The conditions of the flow in a labyrinth seal were rather unexplored. Therefore a more detailed investigation of the size of the dissipative scale was attempted in this work. Its description is given in the next paragraph.

Considering the measurement possibilities in the installation, the standard version of the 'q^2–ϵ' model gives a satisfactory result without adjusting model constants to the conditions in the labyrinth (figures 2 and 3). Suggestions for a special treatment of the turbulence under the influence of swirl or streamline curvature within the two-equation model is based on either a suitable defined Richardson number (Bradshaw

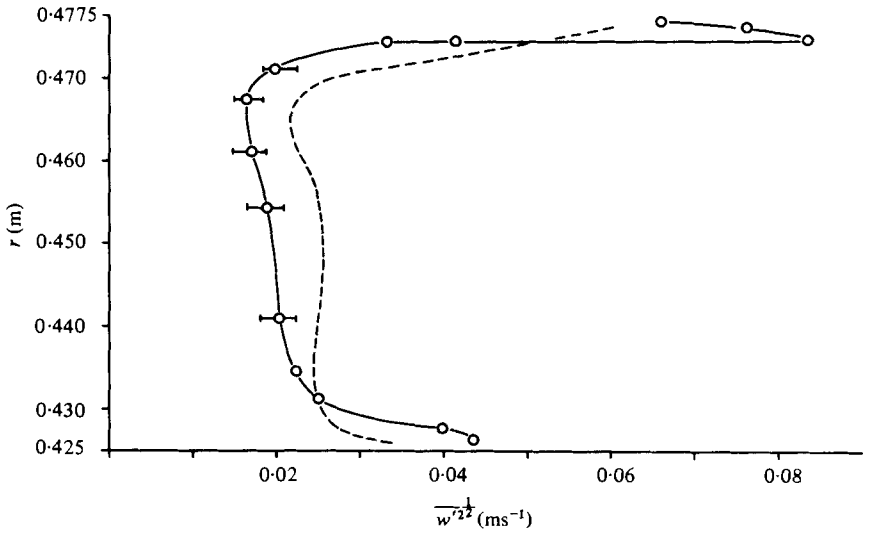

FIGURE 3. Computed (– – –) and measured (—○—) distributions of the r.m.s. value of the circumferential velocity over the radius.

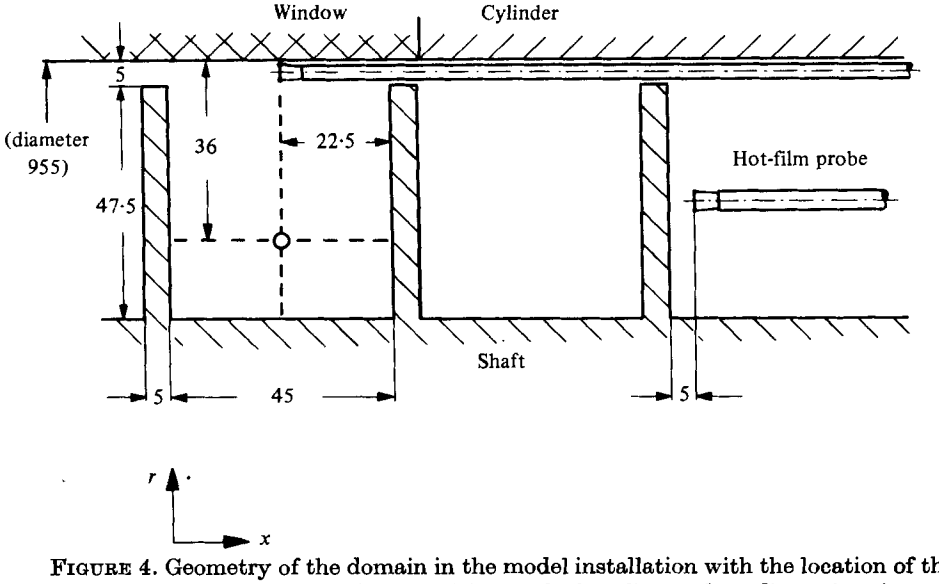

FIGURE 4. Geometry of the domain in the model installation with the location of the laser measurements (– – –) and the position of the hot-film probes (dimensions in mm).

1969; Gosman *et al.* 1976; Johnston 1976; Koosinlin & Lockwood 1974; Lilley 1973; Sharma 1977; So 1978), or on a term involving the fluctuations normal to the wall (Wilcox & Chambers 1977). The latter recommendation creates negative turbulence energy when used with the 'q^2–ϵ' model. The Richardson-number-based swirl correction becomes effective only in the inner part of the boundary layer which is not sufficiently resolved in our computation of the whole domain. More complex modelling of the turbulence structure involves Reynolds stress computation (e.g. Launder, Reece & Rodi 1975) which does not seem to guarantee success within the accuracy of the computational methods available for this case. The main obstacles in the tentative use of

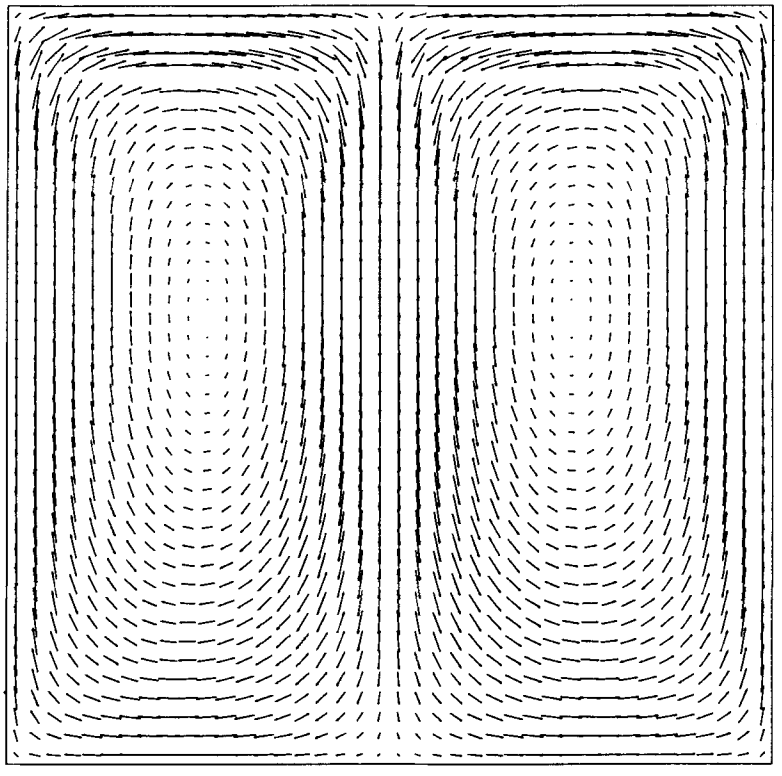

FIGURE 5. Recirculation in the plane of the secondary flow without an imposed axial leakage velocity (grid 40 × 40 points).

algebraic Reynolds stress modelling were lack of convergence in the numerical method and the realizability of a physically meaningful solution of the turbulence energy.

The result obtained with the two-equation 'q^2–ϵ' model exhibits clearly a dependence of the flow pattern on the ratio of axial inlet velocity U_{in} versus circumferential velocity W_{bulk}. In the absence of an axial throughflow, two vortices are generated by the acceleration of the flow close to the revolving baffles (figure 5). When $U_{\text{in}}/W_{\text{bulk}} = 0{\cdot}06$, the two vortices remain existent, but they are dislocated (figure 6). For $U_{\text{in}} > W_{\text{bulk}}$ the flow approaches the case of the driven cavity (figure 7). The computation under operating conditions compares well with the pattern obtained by Boyman & Suter (1978). Experimental investigations in short annuli by Cole (1976) and Benjamin (1978) lend support to the results of this work. Alziary de Roquefort & Grillaud (1978) confirm our secondary-flow solution with their computation in a similar configuration in the absence of axial through-flow.

5. Experimental verification of the dissipation rate ϵ

The experimental verification of the turbulence dissipation rate ϵ is more laborious than that of the kinetic energy $\frac{1}{2}q^2$. Direct measurements of the spatial gradient of the fluctuating velocities in two points were ruled out, because it was not possible to access the flow domain by the two available anemometers at the same time.

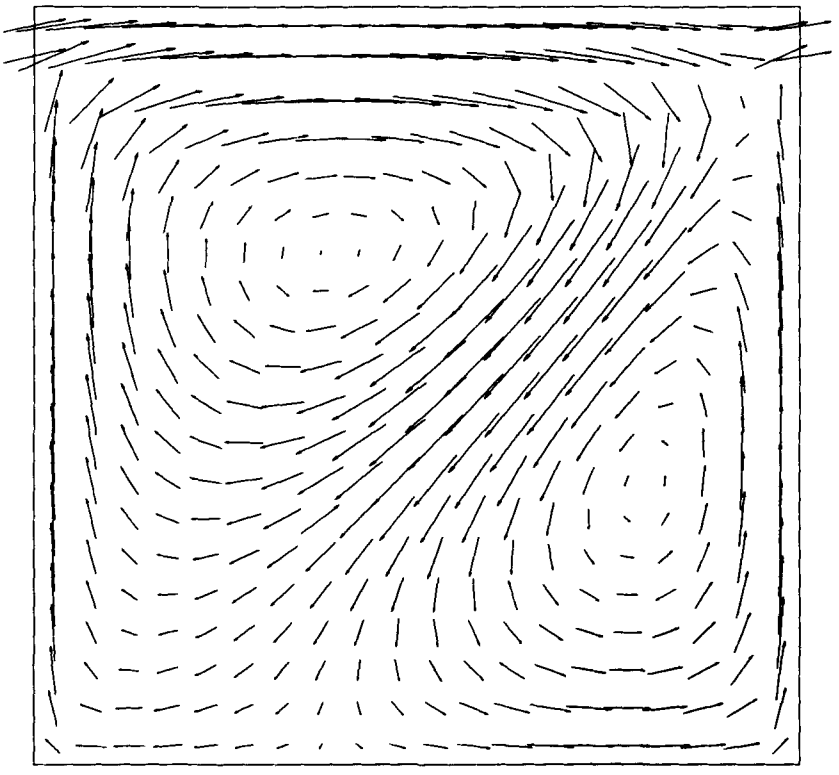

FIGURE 6. Secondary flow field in a grid of 20 × 20 points with a leakage velocity of $U_{in} = 0{\cdot}036\,W_{shaft}$.

Supposing the turbulent fluctuations to be isotropic, which is a reasonable approximation for the inner domain of the labyrinth, two relations allow ϵ to be computed from measurements.

(i) The expression for the isotropic turbulence dissipation as a function of the Taylor microscale.

(ii) The formula for the inertial subrange in the energy spectrum.

(*a*) For the special case of isotropic conditions, the rate of dissipation of turbulence energy can be approximated in the simple form

$$\epsilon = 15\nu\frac{\overline{w'^2}}{\lambda^2}$$

with ν as kinematic viscosity, λ for the Taylor microscale and w' for the circumferential velocity fluctuations (Hinze 1975, p. 219). $\overline{w'^2}$ and λ are accessible to measurements. Two different methods for the quantification of λ were tried.

(i) The microscale λ, defined as a function of the radius of curvature at the beginning of the correlation function R_w, makes it possible to write in our case

$$\lambda_t = 2\Big/\left.\frac{d^2 R_w}{d\tau^2}\right|_{\tau=0} \quad \text{(time scale)},$$

where

$$R_w = \frac{\overline{w'(t)\,.\,w'(t+\tau)}}{\overline{w'^2(t)}}$$

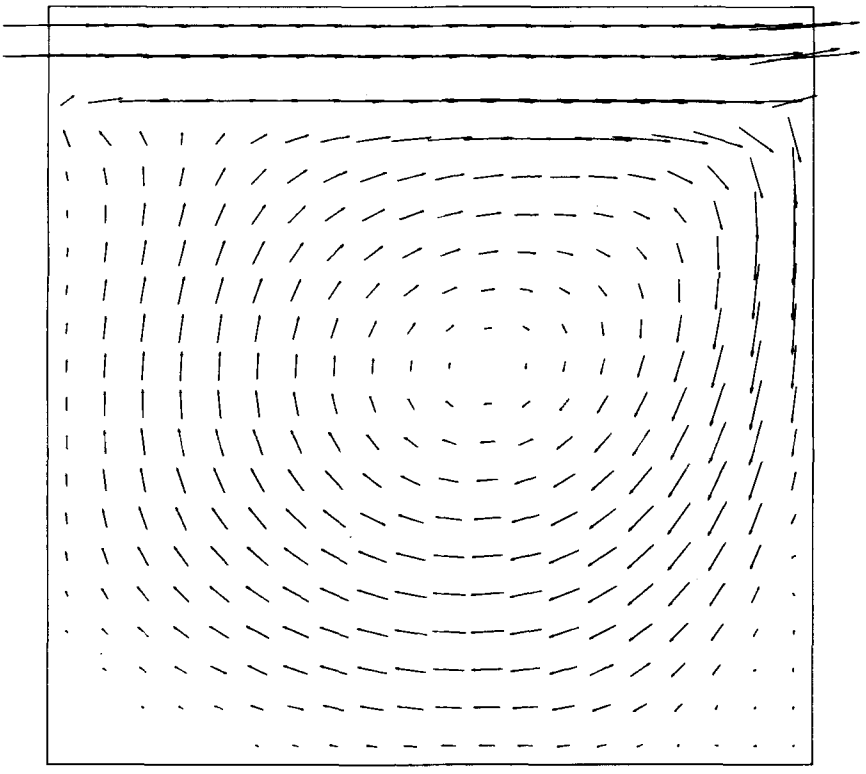

FIGURE 7. Secondary flow pattern in a grid of 20 × 20 points with a leakage velocity of $U_{in} > W_{shaft}$.

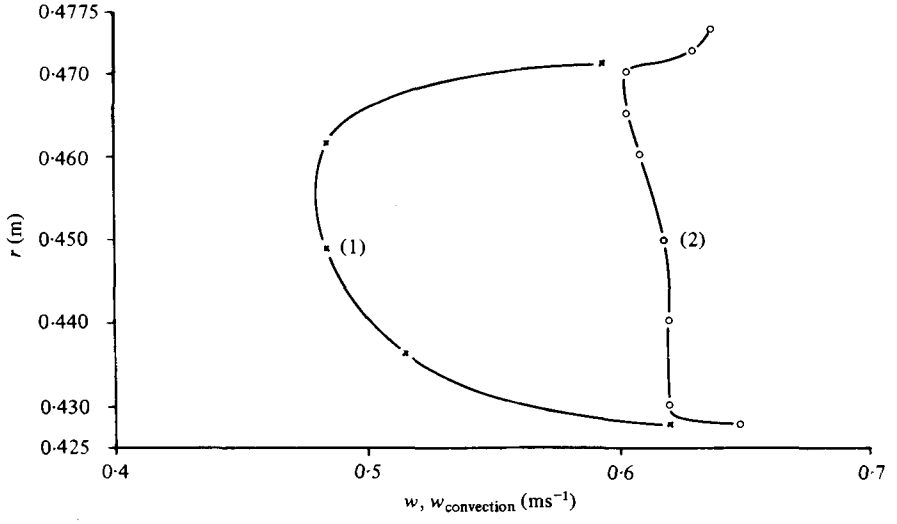

FIGURE 8. Comparison between the convection velocity (1) measured outside the domain with hot film probes and the mean velocity (2) at a corresponding radius inside the domain obtained with a laser–Doppler anemometer (cf. figure 4).

and τ is the correlation time. Taylor's hypothesis of frozen turbulence allows to transform $\lambda = \overline{w}\lambda_t$, though with an error of up to 20 % (figure 8; Rotta 1972, p. 148).

(ii) Another related possibility to establish λ involves the derivative of the velocity (Tennekes & Lumley 1973, p. 211):

$$\lambda_t = \left(2\overline{w'^2} \Big/ \left(\overline{\frac{dw'}{dt}}\right)^2\right)^{\frac{1}{2}}.$$

(*b*) Kolmogorov's second similarity hypothesis predicts a power $(-\frac{5}{3})$ slope in the inertial subrange of the energy spectrum of high-Reynolds-number turbulence ($Re \geqslant 10^4 - 10^5$). The mathematical relation for this subregion gives the kinetic energy E_w of turbulence as a function of the turbulence dissipation ϵ and the wave-number k_w (Lawn 1971):

$$E_w = 0{\cdot}53\epsilon^{\frac{2}{3}}k_w^{-\frac{5}{3}}.$$

This energy spectrum can be visualized directly on commercial spectrum analysers, but it has been found more practical to use the Fourier transformed auto-correlation data from a multichannel analyser (correlator):

$$E_w = \frac{4}{\overline{w}}\int_0^\infty \{R_w(r_w)\cos(k_w r_w)\}\,dk_w,$$

where $r_w = \overline{w}\tau$. The necessary sampling rate is more clearly detectable in the horizontal start of the auto-correlation curve than in the shape of the high-frequency range of the spectrum. The Reynolds number in the labyrinth is at the lower limit of the range of applicability of this spectral procedure, and thus the inertial subrange is not always clearly visible with a constant power $(-\frac{5}{3})$ slope. In such a case ϵ is deduced from the point in the logarithmic spectrum, into which a $(-\frac{5}{3})$ tangent can be fitted.

6. Discrepancies in the dissipation measurements

The auto-correlation function, when measured with a laser of 5 mW (BBC-GOERZ) or 3 W (DISA), shows considerable variations (figure 9). A significant feature is the steep descent of the auto-correlation curves obtained with the 3 W laser–Doppler anemometer. Apparently the strong illumination causes a broadening of the Doppler spectrum towards higher frequencies due to the detection of back-scattering from more than one particle in the control volume. Obviously the measurement of fine-scale turbulence is dependent on the optical conditions: both, the DISA tracker and the BBC-GOERZ tracker, exhibit the same trend in the auto-correlation function when they are used with the 3 W laser. This supports the recommendation of Lawn (1971) for hot-wire measurements in pipe flow, to use rather the inertial subrange of the energy spectrum than the microscale measurement for the determination of ϵ, provided the Reynolds number is above 10^4. Figure 10 demonstrates the result of the dissipation values derived from the measurements and from the 'q^2–ϵ' computation. When looking at the discrepancies, one should keep in mind that the dissipation in general is verified least successfully among the physical variables involved and that also the transport model equation for ϵ is the equation most subject to model assumptions.

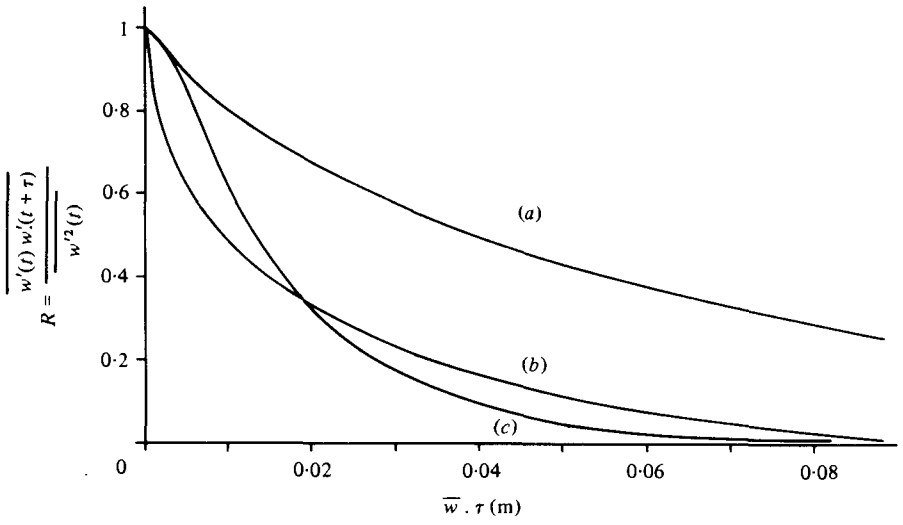

FIGURE 9. Trends in the auto-correlation function measured with: (*a*) LDA BBC–GOERZ and correlator DIDAC 800; (*b*) LDA DISA and correlator HONEYWELL SAI-43A; (*c*) Hot-film anemometer and correlator DIDAC 800.

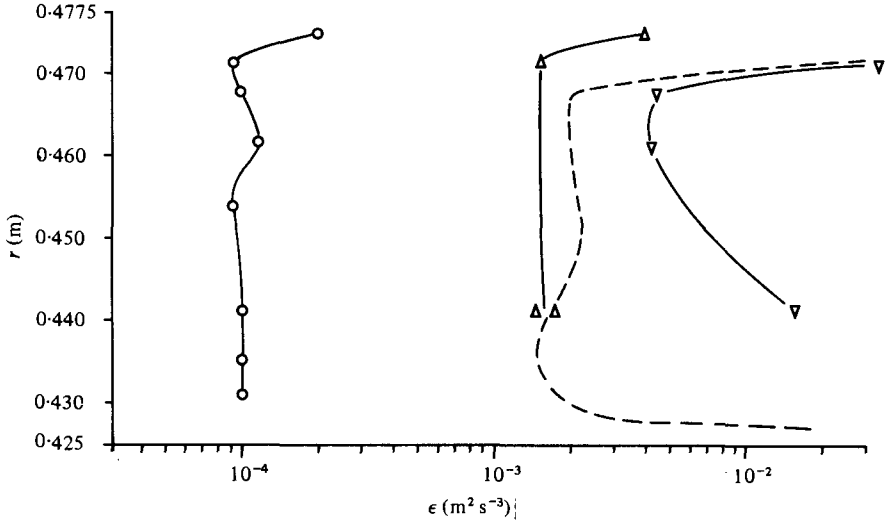

FIGURE 10. Dissipation of turbulence obtained by the energy-dissipation model of turbulence (– – –), and values computed from measured data of the velocity derivative (○) and the energy spectrum (△ = LDA BBC, ▽ = LDA DISA).

7. Conclusions

The finite difference computer program gives a satisfactory answer to the problem of leakage in the labyrinth seal. The influence of the turbulent fluctuations on the mean momentum transport is sufficiently well represented by the two-equation energy-dissipation turbulence model. A more detailed modelling over the entire cavity of the labyrinth does not seem to be justified in connexion with the present numerical solution method.

Laser–Doppler measurements become increasingly difficult close to the solid walls and for components off the circumferential direction, i.e. the principal velocity component. The auto-correlation curves show a dependence on the laser power of the anemometer or the particle concentration. Though the ambiguity effect (cf. George & Lumley 1973) can be excluded, because the fringe system is comparable to the Kolmogorov length scale in size, a broadening of the Doppler spectrum seems to be responsible for the erroneous fine-scale data of turbulence.

I am indebted to Professor P. Suter and to the late Professor F. Baatard from Ecole Polytechnique Fédérale de Lausanne for their help in the accomplishment of this work. Valuable discussions with Professor B. Chaix from Eidgenössische Technische Hochschule Zürich are gratefully acknowledged. Professor D. B. Spalding from Imperial College London kindly allowed me to benefit from his experience in computational methods for turbulent flows.

REFERENCES

ALZIARY DE ROQUEFORT, T. & GRILLAUD, G. 1978 Computation of Taylor vortex flow by a transient implicit method. *Comp. & Fluids* **6**, 259.

BENJAMIN, T. B. 1978 Bifurcation phenomena in steady flows of a viscous fluid. *Proc. Roy. Soc.* A **359**, 27.

BOYMAN, T. 1979 Phénomènes de transport dans les garnitures à labyrinthes des turbomachines. *Communication* no. 7 *de l'Institut de Thermique Appliquée, EPF Lausanne.* (Thesis report.)

BOYMAN, T. & SUTER, P. 1978 Transport phenomena in labyrinth seals of turbomachines. *AGARD Conf. Proc. Seal technology in gas turbine engines, London.*

BRADSHAW, P. 1969 The analogy between streamline curvature and buoyancy in turbulent shear flow. *J. Fluid Mech.* **36**, 177.

COLE, J. A. 1976 Taylor-vortex instability and annulus-length effects. *J. Fluid Mech.* **75**, 1.

DONNELLY, R. J. & SCHWARZ, K. W. 1965 Experiments on the stability of viscous flow between rotating cylinders. *Proc. Roy. Soc.* A **283**, 531.

GEORGE, K. W. & LUMLEY, J. L. 1973 The laser–Doppler velocimeter and its application to the measurement of turbulence. *J. Fluid Mech.* **60**, 321.

GOLLUB, J. P. & SWINNEY, H. L. 1975 Onset of turbulence in a rotating fluid. *Phys. Rev. Lett.* **35**, 927.

GOSMAN, A. D., KOOSINLIN, M. L., LOCKWOOD, F. C. & SPALDING, D. B. 1976 Transfer of heat in rotating systems. *A.S.M.E. public.* 76-GT-25.

GOSMAN, A. D. & PUN, W. 1974 Lecture notes for course entitled 'Calculation of recirculating flows'. *Imperial College London, Mech. Eng. Dept. Rep.* HTS/74/2.

HAKEN, H. 1977 *Synergetics.* Springer.

HINZE, J. O. 1975 *Turbulence*, 2nd edn. McGraw-Hill.

HUTCHINSON, P., KHALIL, E. E., WHITELAW, J. H. & WIGLEY, G. 1976 The calculation of furnace-flow properties and their experimental verification. *Trans. A.S.M.E.* C, *J. Heat Transfer* **98**, 276.

JOHNSTON, J. P. 1976 Internal flows. *Turbulence: Topics in Applied Physics*, vol. 12. (ed. P. Bradshaw), p. 109. Springer.

KOOSINLIN, M. L. & LOCKWOOD, F. C. 1974 The prediction of axisymmetric turbulent swirling boundary layers. *A.I.A.A. J.* **12**, 547.

LAUNDER, B. E., REECE, G. J. & RODI, W. 1975 Progress in the development of a Reynolds-stress turbulence closure. *J. Fluid Mech.* **68**, 537.

LAWN, C. J. 1971 The determination of the rate of dissipation in turbulent pipe flow. *J. Fluid. Mech.* **48**, 477.

LILLEY, D. G. 1973 Prediction of inert turbulent swirl flows. *A.I.A.A. J.* **11**, 955.

LILLEY, D. G. 1976 Computing strongly swirling flows with a primitive pressure-velocity code. *A.I.A.A. J.* **14**, 749.

ROTTA, J. C. 1972 *Turbulente Strömungen*, Stuttgart: Teubner.

SHARMA, B. I. 1977 Computation of flow past a rotating cylinder with an energy-dissipation model of turbulence. *A.I.A.A. J.* **15**, 271.

So, R. M. C. 1978 Turbulent boundary layers with large streamline curvature effects. *Z. angew. Math. Phys.* **29**, 54.

STOFF, H. 1979 Calcul et mesure de la turbulence d'un écoulement incompressible dans le labyrinthe entre un arbre en rotation et un cylindre stationnaire. Report submitted for a doctoral thesis at Ecole Polytechnique Fédérale de Lausanne, no. 342.

TAYLOR, G. I. 1935 Distribution of velocity and temperature between concentric rotating cylinders. *Proc. Roy. Soc.* A **151**, 494 and *The Scientific Papers of Sir G. I. Taylor*, vol. 2 (ed. G. K. Batchelor), Cambridge University Press (1960).

TENNEKES, H. & LUMLEY, J. L. 1973 *A First Course in Turbulence*. Massachusetts Institute of Technology Press.

WILCOX, D. C. & CHAMBERS, T. L. 1977 Streamline curvature effects on turbulent boundary layers. *A.I.A.A. J.* **15**, 574.